Instability of creeping flow past a deformable wall: The role of depth-dependent modulus

Vasileios Gkanis and Satish Kumar*
Department of Chemical Engineering and Materials Science, University of Minnesota, 151 Amundson Hall, 421 Washington Avenue SE, Minneapolis, Minnesota 55455, USA
(Received 31 July 2005; published 15 February 2006)

Linear stability analysis is carried out to examine the effect of a depth-dependent modulus on the stability of creeping flow of a Newtonian fluid past an incompressible and impermeable linear elastic solid. Two different systems are considered: (i) Couette flow past a solid with a continuously varying modulus, and (ii) Couette flow past two adjacent solids with different thicknesses and moduli. For the first system, we find that between two configurations having the same average modulus, the more stable configuration is the one that has the higher modulus at the interface. In the case of two different configurations having the same interfacial modulus and the same average modulus, the more stable configuration is the one that has the higher modulus right below the interface. For the second system, we find that stability depends in a non-monotonic way on the modulus ratio (top modulus to bottom modulus) of the two solids. If the thickness of the top solid is less than a critical value, then increasing the modulus ratio initially causes the system to be less stable. Since this critical thickness decreases as the modulus ratio increases, increasing the modulus ratio beyond a certain point causes the system to be more stable. An analysis of the solid-solid interfacial boundary conditions suggests that the relationship between the stiffness of the top solid and the stability of the system is due to a jump in the base-state displacement gradient at the interface which creates a net perturbation displacement.

DOI: 10.1103/PhysRevE.73.026307 PACS number(s): 47.20.Ma

I. INTRODUCTION

Fluid flows near deformable solids are encountered in numerous applications including microfluidic devices [1,2], membrane separations [3], coating processes [4], oil recovery [5], and flow of biological fluids [6,7]. The physics of such flows can be difficult to analyze due to the coupling between the fluid and the solid dynamics. A particularly important manifestation of this coupling is the ability of the fluid flow to amplify waves at the solid-fluid interface. This instability can happen even when the fluid lacks inertia, and has been a topic of much recent study due to its potential application in mixing, complex fluid rheology, and drag reduction [8–21]. Stability analyses of fluid flows past deformable solids typically assume that the shear modulus of the solid is constant. Yet in practice, the solids may have a modulus that varies with depth, either naturally or by design. For example, vertical gradients in the modulus can form during curing of a polymer gel, or it may be desirable to use a high-modulus protective layer to prevent damage [22]. The purpose of this work is to investigate how a depth-dependent modulus affects the ability of fluid flow to amplify waves at the interface between the fluid and a deformable solid.

The stability of creeping Couette flow past a linear viscoelastic solid was studied by Kumaran *et al.* [8]. They found that an instability occurs when the dimensionless strain $G=\mu V/RE$ is larger than a critical value. Here, μ and R are the fluid viscosity and thickness, respectively, V is the speed of the top plate, and E is the shear modulus of the solid. The critical strain depends on the interfacial tension, the solid-to-fluid viscosity ratio, and the solid-to-fluid thickness ratio. It is important to note that no instability would exist if the solid was rigid, so the instability is a consequence of the deformability of the solid-fluid interface. Gkanis and Kumar studied the stability of creeping Couette flow past a neo-Hookean solid and showed that the results agree with those for a linear elastic solid if the solid-to-fluid thickness ratio is sufficiently large [14]. The difference in the critical conditions for small values of that ratio was attributed to the jump in the first normal stress difference across the interface, which is proportional to G^2 [17]. Further studies have examined the roles of inertia [18–21], fluid elasticity [15,13], and pressure-driven flow [9,17,19,20]. In all of these studies, the shear modulus of the solid is assumed to be constant.

Muralikrishnan and Kumaran [10,11] conducted experiments with a rheometer to validate the theoretical predictions of Kumaran *et al.* [8], and observed a sharp transition in the apparent viscosity at a critical strain. Although the experimental and theoretical critical strains were found to be of the same order of magnitude, the theoretical values were consistently smaller. Eggert and Kumar performed similar experiments using a different fluid-gel system to probe the nonlinear aspects of the instability, observing oscillations and hysteresis in the apparent viscosity [16]. Their results suggested that the instability is subcritical, which is consistent with predictions from a weakly nonlinear stability analysis [12]. Also noteworthy are earlier experiments by Krindel and Silberberg involving flow in a gel-lined tube, where a transition to turbulence was observed at a Reynolds number lower than that for a rigid-walled tube [23].

Many studies have been conducted to explore how deformable solid boundaries can be used to stabilize high-Reynolds-number boundary-layer flows [24,25]. Although the solid is typically modeled as a membrane or as a linear viscoelastic solid of finite thickness and constant modulus, some studies have considered multilayer solids [26,27]. The-

*FAX: (612) 626 7246. Email address: kumar@cems.umn.edu

oretical predictions indicate that a proper choice of the physical properties of the solid layers can significantly reduce the growth rates of boundary-layer instability modes, as well as those of flow-induced instability modes that arise from amplification of waves at the solid-fluid interface.

Although the effect of a depth-dependent modulus on the stability of boundary-layer flows past deformable solids has been examined, its effect on the destabilization of creeping flows has not, and it is this limit that we explore in the present work. To do so, we consider two model systems involving creeping Couette flow of a Newtonian fluid. The first consists of flow past a linear elastic solid with a modulus that varies continuously with depth, and the second consists of flow past two incompressible and impermeable linear elastic solids with different thicknesses and moduli. The governing equations are given in Sec. II, base states are calculated in Sec. III, linear stability analysis is described in Sec. IV, results are reported in Sec. V, and conclusions are given in Sec. VI.

II. GOVERNING EQUATIONS

We consider an incompressible Newtonian fluid residing on top of an incompressible and impermeable linear elastic solid, where the entire configuration resides between two parallel rigid plates. The solid is adhered to the bottom stationary plate whereas the top plate moves with a constant velocity $v_x = V_w$. The solid occupies the region $-HR \leqslant z \leqslant 0$ and the fluid occupies the region $0 \leqslant z \leqslant R$. For the system with two solids having different thicknesses and moduli, the top solid occupies the region $-H_1 R \leqslant z \leqslant 0$ and the bottom solid the region $-HR \leqslant z \leqslant -H_1 R$, where $H > H_1$. In the base state the interface is flat and located at $z=0$. As have prior works (e.g., [8,14,17]), we focus our efforts here on two-dimensional systems and suppress any variations in the y direction.

The motion of each medium is governed by a momentum balance and an incompressibility constraint. In the absence of inertia these equations take the form:

$$\nabla \cdot \boldsymbol{\tau} = \mathbf{0}, \tag{1}$$

$$\nabla \cdot \boldsymbol{\Pi} = \mathbf{0}, \tag{2}$$

where $\boldsymbol{\tau}$ is the Cauchy stress tensor in the fluid or the solid and $\boldsymbol{\Pi}$ is the velocity vector in the fluid or the displacement vector in the solid. Henceforth, $\boldsymbol{\tau}$ and $\boldsymbol{\sigma}$ are used to denote the Cauchy stress tensor in the fluid and the solid, respectively. For the system with a continuously varying modulus, $\boldsymbol{\sigma}$ is equal to

$$\boldsymbol{\sigma} = -P_s + [E_o + \hat{E}(z)][\nabla \mathbf{u} + (\nabla \mathbf{u})^T], \tag{3}$$

and it is equal to

$$\boldsymbol{\sigma} = -P_s + E_j[\nabla \mathbf{u} + (\nabla \mathbf{u})^T] \tag{4}$$

for the system with two solids having different thicknesses and moduli, where $j=1,2$. Here, the subscript 1 is for the top layer and the subscript 2 is for the bottom layer. The variable P_s is the pressure in the solid, $E_o + \hat{E}(z)$ is the modulus gradient function, E_j is the modulus of each layer, and $\boldsymbol{u}$ is the displacement vector in the solid.

The governing equations are non-dimensionalized by scaling length with R, pressure with E^* (E^* is equal to E_o for the system with a modulus gradient and it is equal to E_2 for the system with two solids), and time with μ_f / E^*. According to this scaling, the inertial terms in the fluid are multiplied by the term $\mathcal{R} = \rho_f E^* R^2 / \mu_f^2$, and by the term $\rho_s \mathcal{R} / \rho_f$ in the solids. Here, μ_f and ρ_f are the fluid viscosity and density, respectively, and ρ_s is the solid density. We assume that the fluid and the solid densities are comparable and consider the limit of vanishing $\mathcal{R}$. For the system with two solids, the above scaling introduces a new parameter $E_r = E_1 / E_2$, which is the ratio of the moduli of the two layers. Henceforth, all the variables are dimensionless.

The scaled governing equations are solved with the following boundary conditions. At the top plate we have no slip:

$$\boldsymbol{v} = G\boldsymbol{i}, \tag{5}$$

where $G = \mu_f V_w / R E^*$ and $\boldsymbol{i}$ is the unit vector in the x direction. The parameter G can be interpreted as a dimensionless imposed velocity or shear stress. It is also proportional to the strain imposed in the base state on the system under study. Note that $\mathcal{R} = \mathrm{Re}/G$, where $\mathrm{Re} = \rho_f V_w R / \mu_f$ is the Reynolds number. At the bottom plate, there is no displacement:

$$\boldsymbol{u} = \mathbf{0}. \tag{6}$$

At the solid-fluid interface, continuity of velocities and forces holds:

$$\boldsymbol{v} = \frac{\partial \boldsymbol{u}}{\partial t}, \tag{7}$$

$$\boldsymbol{n} \cdot \boldsymbol{\tau} = \boldsymbol{n} \cdot \boldsymbol{\sigma}, \tag{8}$$

where $\boldsymbol{n}$ is the normal vector to the interface. For the system with two solids, we apply continuity of displacements and forces at the solid-solid interface:

$$\boldsymbol{u}_1 = \boldsymbol{u}_2, \tag{9}$$

$$\boldsymbol{n} \cdot \boldsymbol{\tau}_1 = \boldsymbol{n} \cdot \boldsymbol{\tau}_2. \tag{10}$$

Interfacial tension and solid viscosity have not been included in the above equations and boundary conditions. Previous studies involving flow past deformable solids with a constant modulus have shown that both of these quantities have a stabilizing effect [8,14], and we expect the same to be true for the systems studied here.

III. BASE STATE

In the base state there are no disturbances and the interface is flat. Consequently, the continuity of velocity equation (7) becomes $\boldsymbol{v} = \mathbf{0}$. Under these boundary conditions, a Couette flow develops in the fluid. In the solid, the displacement in the x direction varies linearly in the z direction for the system with two solids. The modulus ratio changes the slope of this variation as we go from the top layer to the bottom

layer. For the system with a continuously varying modulus, the displacement in the x direction depends on z in a way determined by the depth-dependent modulus $E(z)$, where $E(z)=\hat{E}(z)/E_o$. That is, we have

$$\frac{\partial u_x}{\partial z}=\frac{G}{1+E(z)}. \tag{11}$$

To solve the differential equation (11), we apply the zero-displacement boundary condition at the bottom plate. For both systems we study, the base-state pressure in the solids is constant and equal to the pressure in the fluid, and $u_z=0$ in the base state.

An important consequence of the linearity of the governing equations is that the coupling between the base state and perturbation quantities will occur only through the interfacial boundary conditions, specifically the x component of the continuity-of-velocity boundary condition (and the continuity-of-displacement boundary condition for the system with two solids). The use of a nonlinear constitutive equation (e.g., the neo-Hookean model) would introduce additional couplings, such as one involving a first normal stress difference that can give rise to a shortwave instability [14,17]. Although linear elastic models are, strictly speaking, valid only for small displacement gradients, $G\ll 1$, they have been shown to provide reasonable predictions for Couette flow past a deformable solid of uniform modulus even when $G\sim 1$ [14]. We expect that this will also hold for flow past a solid with a depth-dependent modulus.

IV. LINEAR STABILITY ANALYSIS

A linear stability analysis is carried out to determine the stability of the base state to small-amplitude disturbances. In Ref. [8], one can find (i) the governing equations for the disturbances in the fluid with the boundary conditions at the top plate, (ii) the boundary conditions for the disturbances at the solid-fluid interface for a solid having a constant modulus, (iii) the governing equations for the disturbances in the solids when each solid has a constant modulus, and (iv) the boundary conditions for the disturbances at the bottom plate. Thus, we do not repeat these here.

Here, we give the solid-solid interfacial boundary conditions for the disturbances for the system with two solids, and the governing equations for the disturbances in the solid with the solid-fluid interfacial boundary conditions for the system with a continuously varying modulus. The interfacial boundary conditions at the solid-solid interface are Taylor expanded around a flat interface, i.e., around $z=-H_1$:

$$\tilde{u}_{z1}=\tilde{u}_{z2}, \tag{12}$$

$$\frac{G}{E_r}\tilde{u}_{z1}+\tilde{u}_{x1}=G\tilde{u}_{z2}+\tilde{u}_{x2}, \tag{13}$$

$$E_r\left(\frac{\partial\tilde{u}_{x1}}{\partial z}+ik\tilde{u}_{z1}\right)=\frac{\partial\tilde{u}_{x2}}{\partial z}+ik\tilde{u}_{z2}, \tag{14}$$

$$-\tilde{P}_{s2}+2\frac{\partial\tilde{u}_{z2}}{\partial z}=-\tilde{P}_{s1}+2E_r\frac{\partial\tilde{u}_{z1}}{\partial z}, \tag{15}$$

where k is the real-valued wave number and the tilde indicates the complex-valued amplitude of the disturbance, which depends on depth. Equations (12) and (13) represent continuity of displacement in the z and x directions, respectively, and Eqs. (14) and (15) represent continuity of forces in the tangential and in the normal directions, respectively.

The governing equations for the disturbances in the solid with a continuously varying modulus are

$$-ik\tilde{P}_s+\frac{\partial E(z)}{\partial z}\left(ik\tilde{u}_z+\frac{\partial\tilde{u}_x}{\partial z}\right)+[1+E(z)]\left(-k^2\tilde{u}_x+\frac{\partial^2\tilde{u}_x}{\partial z^2}\right)=0, \tag{16}$$

$$-\frac{\partial\tilde{P}_s}{\partial z}+2\frac{\partial E(z)}{\partial z}\frac{\partial\tilde{u}_z}{\partial z}+[1+E(z)]\left(-k^2\tilde{u}_z+\frac{\partial^2\tilde{u}_z}{\partial z^2}\right)=0, \tag{17}$$

$$ik\tilde{u}_x+\frac{\partial\tilde{u}_z}{\partial z}=0, \tag{18}$$

where the first two equations are the momentum balances in the x and z directions, respectively, and the third equation is the incompressibility constraint. The solid-fluid interfacial boundary conditions are Taylor expanded around a flat interface, $z=0$, to become

$$\alpha\tilde{u}_z=\tilde{v}_z, \tag{19}$$

$$\alpha\tilde{u}_x=\tilde{v}_x+G\tilde{u}_z, \tag{20}$$

$$-\tilde{P}_s+2[1+E(0)]\frac{\partial\tilde{u}_z}{\partial z}=-\tilde{P}_l+\frac{\partial\tilde{v}_z}{\partial z}, \tag{21}$$

$$[1+E(0)]\left(\frac{\partial\tilde{u}_x}{\partial z}+ik\tilde{u}_z\right)=\frac{\partial\tilde{v}_x}{\partial z}+ik\tilde{v}_z, \tag{22}$$

where α is the complex-valued growth rate. The first two equations represent continuity of velocity and the second two represent continuity of forces.

Equations (16)–(18) can be combined into a linear fourth-order differential equation for $\tilde{u}_z$. A similar equation can be obtained for $\tilde{v}_z$, which has constant coefficients and can be solved analytically. For the system with two solids, the differential equations for $\tilde{u}_z$ have constant coefficients and can also be solved analytically. For the system with a continuously varying modulus, however, the coefficients are not constant and numerical solution of the differential equation is required. The characteristic equation for the growth rate is obtained using the method described in Ref. [17]. For both systems studied, the characteristic equation is quadratic in the growth rate. We found that one root of this equation always has a negative real part, whereas the other root can have a positive real part depending on the problem parameters. If the real part of this root is positive, the system is unstable, if it is negative the system is stable, and if it is zero

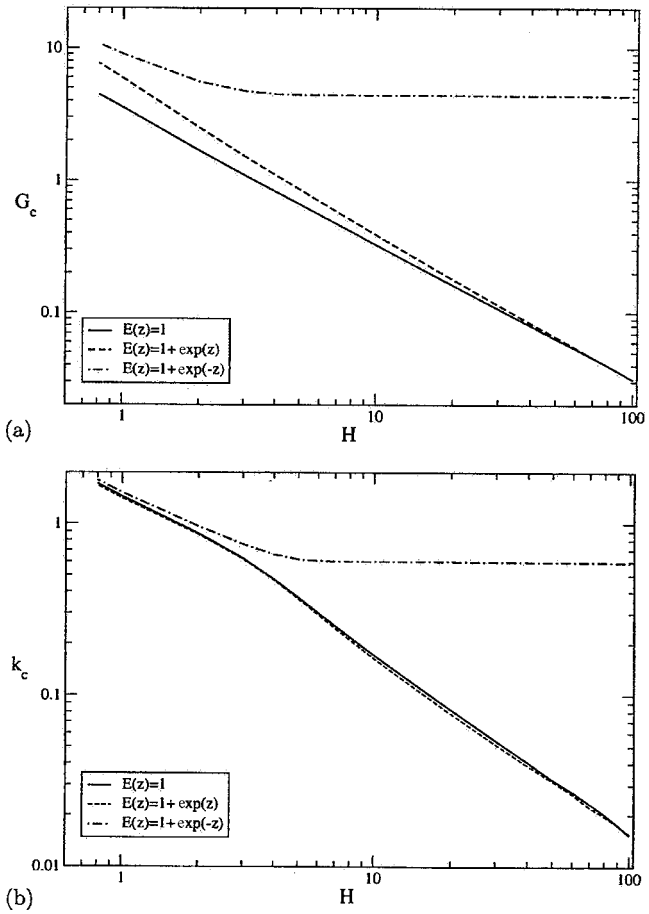

FIG. 1. Plot of (a) G_c and (b) k_c versus H for three different modulus functions: constant, exponentially decreasing, and exponentially increasing.

the system is neutrally stable. Plots of the growth rate versus the wavenumber can be made for different values of G (with the other parameters fixed), and the smallest value of G for which the maximum growth rate is zero is referred to as the critical strain G_c, because for $G > G_c$ the system will be unstable. The corresponding value of k is the critical wave number k_c. In what follows, we discuss the behavior of G_c as a function of the other problem parameters.

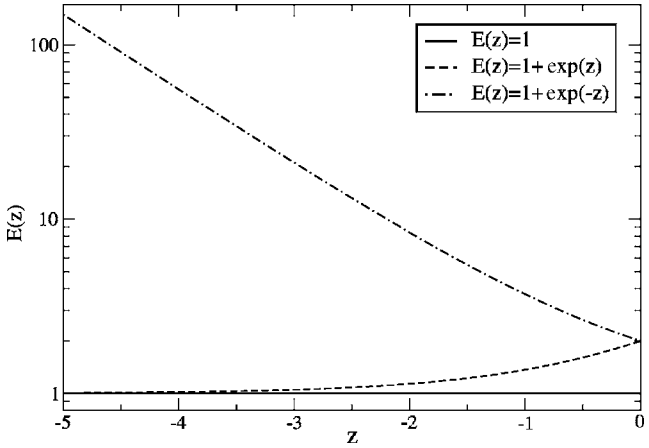

FIG. 2. Modulus of the three functions of Fig. 1 versus depth for $H=5$.

TABLE I. Critical conditions for the linear and exponential modulus functions with the same average modulus and same modulus at the interface.

Modulus function	G_c	k_c	$E(-H)$
Linear	5.722	0.921	6.000
Exponential	5.404	0.957	7.711

V. RESULTS

A. Solid with a continuously varying modulus

In Fig. 1, we plot the critical strain G_c and the corresponding critical wave number k_c versus the solid-to-fluid thickness ratio H for three different modulus functions: constant, exponentially decreasing, and exponentially increasing. As expected, the most stable case is the one where the modulus increases with depth. If we compare Fig. 1 with Fig. 2, where we plot the modulus for these three functions versus depth for $H=5$, we observe two important features. First, when the modulus at the bottom plate is the same, the more stable case is the one with the largest modulus at the interface. Second, when the modulus at the interface is the same, the more stable case is the one with the largest modulus at the bottom plate. However, here we are comparing G_c for systems which do not have the same average modulus. So, to better understand the importance of the value of the modulus at the interface or at the bottom plate, we consider two more modulus functions with the same average modulus and the same modulus at the interface or at the bottom plate.

In Tables I and II, we give the critical conditions for two different modulus functions, linear and exponential, when these functions have the same value at the interface (Table I) or at the bottom plate (Table II). The thickness of the solid is $H=2$, the average modulus is $\bar{E}=2$, and the modulus at the interface (Table I) or at the bottom plate (Table II) is 2. In Fig. 3 we plot these functions versus depth. By comparing G_c for the cases with the same modulus at the bottom plate, we see that the more stable one is that with the exponential variation in the modulus, which also has the higher modulus at the interface. Furthermore, in Table III we give the critical strain and the modulus at the two ends for an exponential modulus function of the form $E(z)=1+a_1\exp(a_2 z)$, where we choose different values for the parameters a_1 and a_2. The

TABLE II. Critical conditions for the linear and exponential modulus functions with the same average modulus and same modulus at the bottom plate.

Modulus function	G_c	k_c	$E(0)$
Linear	6.844	0.836	6.000
Exponential	6.893	0.841	7.711

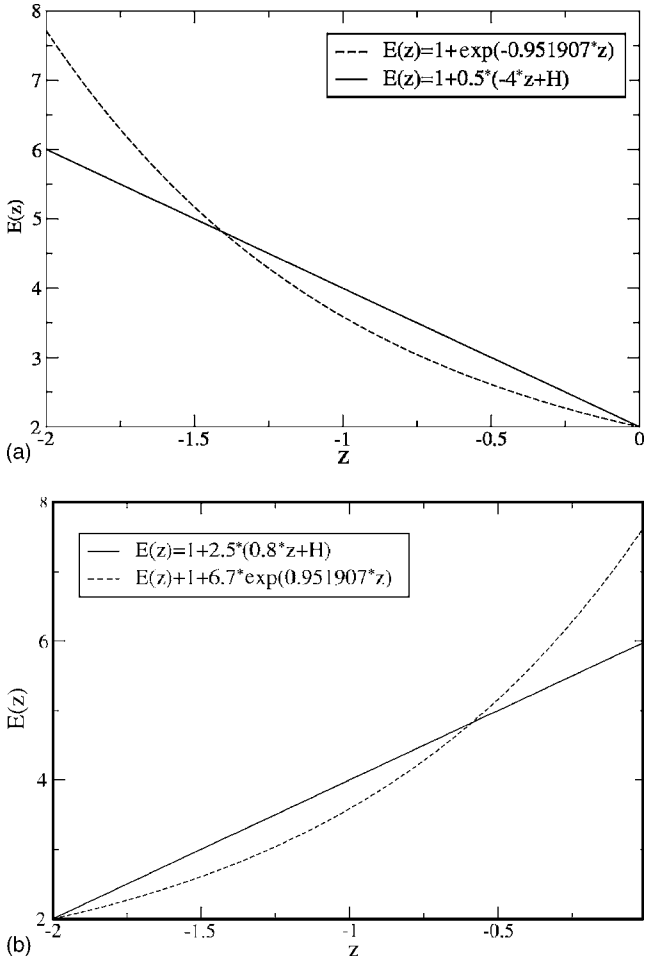

FIG. 3. Modulus versus depth for the case where the modulus at the (a) interface or (b) bottom plate is the same. Here, $H=2$ and $\bar{E}=2$.

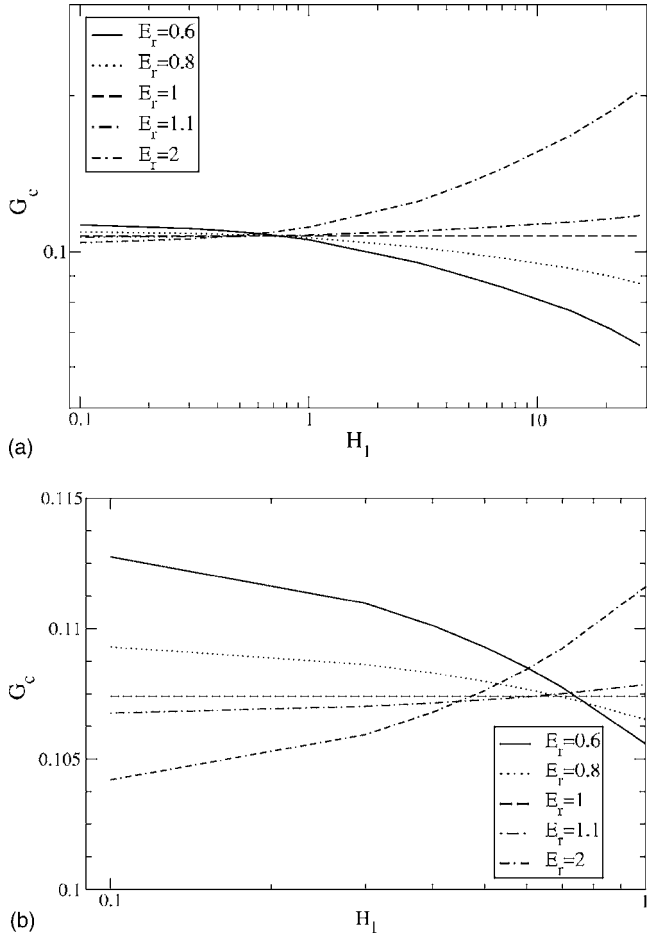

FIG. 4. Plot of G_c versus H_1, for different values of E_r when $H=30$. In (b) we have focused in on the region $0.1 \leqslant H_1 \leqslant 1$.

most stable case is the one where the modulus at the interface is highest, despite the fact that this is the one that also has the lowest modulus at the bottom plate. Therefore, from these observations we conclude that the value of the modulus at the interface is the one that determines stability: the higher it is, the more stable the system is.

When the modulus at the interface is the same (Table I) and the average modulus is the same, the linear modulus function is the more stable one even though it has a lower modulus at the bottom plate. This is because this function has a higher modulus right below the interface, whereas the exponential one has a higher modulus closer to the bottom plate (Fig. 3). To support this idea, we considered different systems where the point at which the two modulus functions have the same value ($\sim$1.5 units from the interface) is closer to the interface, and we found that even if that point is very close to the interface (the smallest distance from the interface was 0.01 units, when the solid thickness was 2 units), the system which has the higher modulus right below the interface is the more stable one.

TABLE III. Critical strain and modulus values at interface and bottom plate for different exponential functions having the same average modulus.

G_c	$E(0)$	$E(-H)$
3.416	2.400	1.685
3.381	2.200	1.824
3.332	2.000	2.000
3.301	1.900	2.107
3.222	1.700	2.376

It is important to emphasize that although the results in this section are consistent with what we might expect, their deduction from existing results on systems where the modulus is constant is far from obvious. This is due to the more complicated mathematical problem that arises when the modulus varies with depth, which involves the numerical solution of an ordinary differential equation with nonconstant coefficients (cf. Sec. IV).

B. Two solids with different thicknesses and moduli

In Fig. 4, we plot G_c versus the thickness of the top layer, H_1, for different values of the modulus ratio E_r $(=E_1/E_2)$. The total thickness is $H=30$. The first thing we notice is that if the top layer is stiffer than the bottom layer, $E_r>1$, G_c

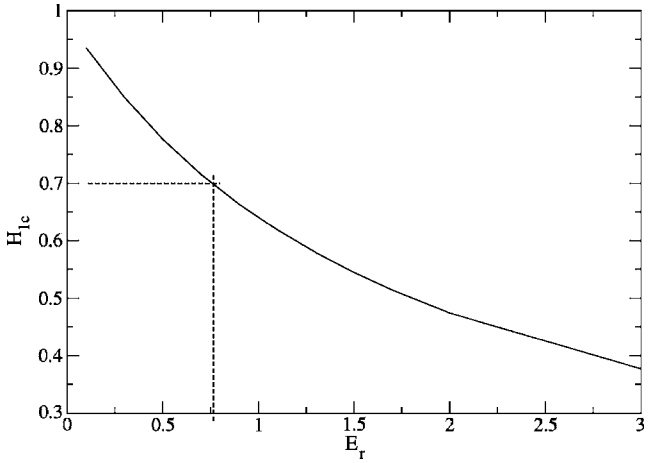

FIG. 5. The critical thickness of the top layer, H_{1c}, versus E_r when $H=30$. The dashed lines indicate the value of E_r ($E_r \sim 0.8$) for which $H_{1c}=0.7$.

increases with increasing H_1. On the other hand, if the top layer is softer than the bottom layer, $E_r<1$, then G_c decreases with increasing H_1. The interesting things occur when $H_1<1$ [Fig. 4(b)], where we see that by increasing the stiffness of the top layer, we decrease G_c. Thus, the stiffer the top layer is, the easier it is to destabilize the system. Moreover, in Fig. 4(b) we observe that the lines which correspond to different values of E_r cross the line that corresponds to a single layer, $E_r=1$. This means that there is a critical thickness of the top layer, H_{1c}, such that G_c for a system with $E_r \neq 1$ is equal to G_c for a single layer system ($E_r=1$). Referring back to Fig. 4, we see that for $H_1<H_{1c}$, a top layer stiffer (softer) than the bottom layer makes the system less (more) stable, and for $H_1>H_{1c}$, a stiffer (softer) top layer makes the system more (less) stable. It is helpful to note here that according to the scaling used, the dimensionless modulus of the bottom layer is 1; similarly, the dimensionless modulus of a system with a single layer of constant modulus is also 1.

The critical thickness of the top layer decreases monotonically with E_r, as is shown in Fig. 5. In Fig. 6, we plot G_c

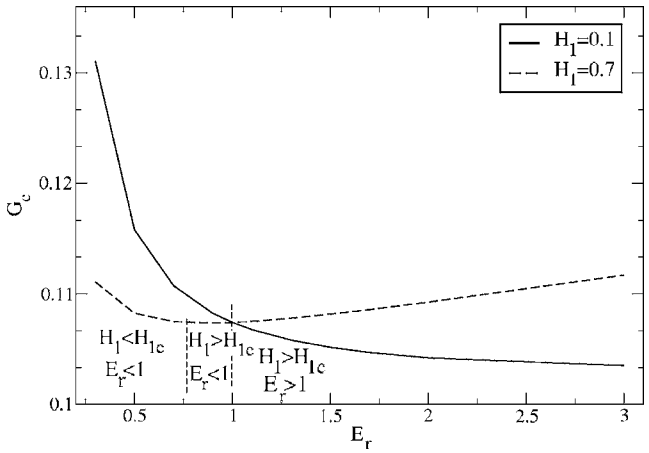

FIG. 6. Plot of G_c versus E_r for $H_1=0.1$ and $H_1=0.7$ when $H=30$. The first vertical dashed line indicates the point where $E_r=0.8$ and the second line the point where $E_r=1$.

TABLE IV. Comparison of the critical conditions for the two systems

	Continuously varying modulus		Two solids	
H_1	G_c	k_c	G_c	k_c
0.1	0.108	0.054	0.104	0.055
0.5	0.112	0.053	0.108	0.053
14.0	0.169	0.055	0.168	0.055

versus E_r for two different values of H_1, when the total thickness is $H=30$. We observe that G_c goes through a minimum when $H_1=0.7$ and it decreases monotonically when $H_1=0.1$. This behavior can be explained with the help of Figs. 4 and 5. From Fig. 5, we have that $H_{1c}>H_1$ for all the values of E_r examined in this work when $H_1=0.1$. Therefore, we have a top layer with a thickness smaller than the critical thickness and the stiffer we make that layer, the easier it is to destabilize the system. Of course, if E_r becomes sufficiently large, H_{1c} will eventually drop below $H_1=0.1$, and increasing E_r further will then begin to increase G_c. We also note that according to the discussion of Fig. 4(b), G_c is larger when $E_r<1$ (and $H_{1c}>H_1$) than when $E_r=1$. The reverse holds for $E_r>1$. This explains why G_c for $0.1<E_r<1$ ($1<E_r<3$) is larger (smaller) than G_c for a single layer, $E_r=1$.

When $H_1=0.7$, we find that the critical thickness $H_{1c}=0.7$ when $E_r \sim 0.8$, as is shown in Fig. 5. According to this figure, if $E_r<0.8$ then $H_{1c}>H_1$ and the reverse holds when $E_r>0.8$. Therefore, for $E_r<0.8$ we have a soft top layer with a thickness smaller than the critical thickness and hence G_c is larger than it would be when $E_r=1$. However, G_c decreases as we stiffen the top layer [Fig. 4(b)]. For $0.8 \leqslant E_r \leqslant 1$, $H_1>H_{1c}$, and because $E_r<1$, G_c is smaller than its value when $E_r=1$. Nevertheless, because now $H_1>H_{1c}$, G_c increases as we stiffen the top layer. This means that G_c has a minimum when $E_r=0.8$. For $E_r>1$ we observe behavior consistent with Fig. 4 when $E_r>1$ and $H_1>H_{1c}$, i.e., G_c increases with E_r.

We next present the critical conditions for Couette flow past a linear elastic solid with a modulus function of the form $E(z)=a_1+a_2 \arctan(a_3 z+a_4)$, where the values of the a_i ($i=1,\ldots,4$) control the steepness of the function and its values at the two ends. The values of the a_i were chosen to make the arctan function look like the step function seen in the case where there are two solids of different moduli. The values of G_c and k_c reported for the arctan function did not change much upon increasing the steepness of that function. Our motivation for studying this function was to check whether we could reproduce some of the results reported in this section using a single solid with a continuously varying modulus. In Table IV we give the critical conditions for different values of H_1. The total thickness is $H=30$ and the modulus ratio is $E_r=2$. There is a good agreement for large values of H_1, and for both systems G_c decreases as H_1 decreases. Nevertheless, for the system of a single solid with a modulus gradient, G_c is not smaller than the critical imposed velocity for a single layer with constant modulus ($G_c=0.107\,41$), although G_c is smaller for the system with two solids. We believe that some insight into this can be

gained by examining the solid-solid interfacial boundary conditions. Equation (13) shows that the jump in the displacement gradient in the base state produces a net perturbation displacement in the x direction. That is, Eq. (13) can be written as

$$\tilde{u}_{x1} - \tilde{u}_{x2} = \left(\frac{\partial}{\partial z}(u^o_{x2} - u^o_{x1}) \bigg|_{z=-H_1} \right) \tilde{u}_{z2} = (G - G/E_r)\tilde{u}_{z2}, \tag{23}$$

where the superscript o denotes the base state. A nonzero difference of $\tilde{u}_{x1} - \tilde{u}_{x2}$ indicates a net perturbation displacement in the x direction at the solid-solid interface. If we set the right hand side of Eq. (23) to zero:

$$\tilde{u}_{x1} - \tilde{u}_{x2} = 0, \tag{24}$$

and use this to calculate the critical conditions, we recover the results we obtain with the arctan function. Thus, the net perturbation displacement at the interface appears to be responsible for the differences we observe in Table III.

Further consideration of Eq. (23) can also yield insight into the relationship between stiffness and stability observed in Fig. 4. The term $(G - G/E_r)$ in Eq. (23) is positive when $E_r > 1$ (stiffer top layer) and negative when $E_r < 1$ (stiffer bottom layer). We adopt the convention that the magnitude and the sign of the net perturbation displacement are determined by the term $(G - G/E_r)$; when that term is positive (negative), Eq. (23) produces a net perturbation displacement to the right (left). In our analysis we also consider continuity of velocity, Eq. (20), at the solid-fluid interface, which indicates that a jump in the velocity gradient in the base state produces a net perturbation flow. (In the base state, the velocity in the solid is zero, but it is a function of position in the fluid.) Equation (20) is $\partial \tilde{u}_x / \partial t - \tilde{v}_x = v^o_x(\tilde{u}_{z1})$, and after Taylor expanding around $z=0$, it becomes $\partial \tilde{u}_x / \partial t - \tilde{v}_x = (\partial v^o_x / \partial z)|_{z=0} \tilde{u}_{z1} = G\tilde{u}_{z1}$. So the net perturbation flow is proportional to G, a positive parameter, and hence according to the previous convention, that flow is to the right. To summarize, the solid-fluid interface is shifted to the right and the solid-solid interface is shifted to the right or left according to the sign of the term $(G - G/E_r)$. Moreover, it was noted earlier that the modulus of the bottom layer is equal to the modulus of the system with a single layer, and from prior work [8,17] it is known that the motion of the solid-fluid interface is the one that drives the instability. In this analysis, we will consider only the effect of the thickness of the top layer on the stability of the system.

In the case where the modulus ratio is less than unity, the solid-fluid interface is shifted to the right and the solid-solid interface is shifted to the left. Because these two interfaces are moving in the opposite directions, the motion of the solid-solid interface may counterbalance the destabilizing motion of the solid-fluid interface, making the system more stable than that of a single layer. This corresponds to what happens when $H_1 < H_{1c}$ [Fig. 4(b) when $E_r < 1$]. Nevertheless, as the thickness of the top layer increases such that $H_1 > H_{1c}$, these two interfaces move farther away one another so that the motion of one interface does not affect the motion of the other. Moreover, because the top layer has a lower modulus, $E_r < 1$, its resistance to deformation is smaller than that of the bottom layer and hence it is easier to destabilize this system than one having a single layer [Fig. 4(a) when $E_r < 1$ and $H_1 > H_{1c}$]. Similar reasoning applies to the case of $E_r > 1$. Now, both interfaces are shifted to the right and hence the destabilizing motion of the solid-fluid interface is reinforced by the motion of the solid-solid interface. The system is less stable than the system of a single layer [Fig. 4(b) when $E_r > 1$]. On the other hand, when $H_1 > H_{1c}$ the two interfaces are far away one from the other so that the motion of one interface does not affect the motion of the other. Furthermore, the solid-fluid interface has to deform the stiffer top layer, something that makes the system more stable than a system consisting of a single layer [Fig. 4(a) when $E_r > 1$ and $H_1 > H_{1c}$].

In the case where we keep the thickness of the top layer constant and we decrease its modulus, the stress in the solid is smaller for a given strain. This means that the stress exerted on one interface due to the motion of the other interface is now smaller. Therefore, it would appear that the solid-solid interface has a smaller stabilizing effect (if $E_r < 1$) or a smaller destabilizing effect (if $E_r > 1$) than it has for a larger modulus. But in this case the situation is more complex because the net perturbation displacement is a function of the modulus (it is proportional to $G - G/E_r$), and this will also affect the magnitude of the stress on the solid-fluid interface. Thus, changes in the net perturbation displacement might compensate for changes in the modulus, and this may give rise to the observed dependence of H_{1c} on E_r (Fig. 5) and G_c on E_r (Fig. 4).

VI. CONCLUSIONS

In this work, we carried out a linear stability analysis for two systems involving creeping Couette flow of a Newtonian fluid past a linear elastic solid with a depth-dependent modulus. For the system where the modulus varies continuously with depth, we found that stability is governed by the value of the modulus at the interface; the greater it is, the more stable the system is. In the case of different configurations having the same interfacial modulus and the same average modulus, the more stable configuration is the one that has the higher modulus right below the interface. For the system with two solids having different thicknesses and moduli, the critical strain required for instability is a nonmonotonic function of the modulus ratio. The critical strain required for instability decreases as the top layer becomes stiffer, provided that its thickness is below a critical value. Since this critical value decreases as the modulus ratio increases, making the top layer too stiff eventually causes the critical strain to increase. Analysis of the solid-solid interfacial boundary conditions suggests that this behavior is due to a net perturbation displacement at the interface which arises due to a jump in the base-state displacement gradient across the interface. We note that our results should also be valid for pressure-driven flows, as the form of the linearized equations will be the same with only a different effective value of G.

The results presented in this work significantly extend prior work on the stability of creeping flows past deformable

solids by elucidating the effect of a depth-dependent modulus. As most soft elastic solids will have a modulus gradient, our results may be helpful in interpreting experimental data. Although we are not aware of experimental studies with which we can quantitatively compare our results, it is intriguing to reconsider the experimental observations on low-Reynolds-number flow past polymer gels [10,11]. It was found that although linear stability analysis using a linear viscoelastic model with constant modulus predicts critical strains of the same order of magnitude as the experimental values, the theoretical values are consistently smaller. The results of the present work suggest that the discrepancy could be due to a depth-dependent modulus. As polymer gels cure, they can develop a modulus gradient through their depth due to differences in cross-link density, where the modulus is highest near the top surface [22]. It is possible that the gels used in the experiments also had a higher modulus near the surface, although no measurements of modulus versus depth were made. If so, then our results suggest that the observed values of the critical strain would be expected to be larger than those predicted by a constant-modulus model.

ACKNOWLEDGMENTS

Acknowledgment is made to the Donors of the The American Chemical Society Petroleum Research Fund for partial support of this research. S.K. also thanks the Shell Oil Company Foundation for support through its Faculty Career Initiation Funds program, and 3M for a Nontenured Faculty Award. We are grateful for resources from the University of Minnesota Supercomputing Institute.

[1] S. R. Quake and A. Scherer, Science **290**, 1536 (2000).
[2] G. M. Whitesides and A. D. Stroock, Phys. Today **54**(2), 42 (2001).
[3] P. A. Belter, E. L. Cussler, and W.-S. Hu, *Bioseparations* (Wiley, New York, 1988).
[4] M. S. Carvalho and L. E. Scriven, J. Comput. Phys. **138**, 449 (1997).
[5] T. P. Lockhart and E. Borgarello, Prog. Colloid Polym. Sci. **109**, 49 (1998).
[6] J. B. Grotberg and O. E. Jensen, Annu. Rev. Fluid Mech. **36**, 121 (2004).
[7] J. A. Moriarty and J. B. Grotberg, J. Fluid Mech. **397**, 1 (1999).
[8] V. Kumaran, G. H. Fredrickson, and P. Pincus, J. Phys. II **4**, 893 (1994).
[9] V. Kumaran, J. Fluid Mech. **294**, 259 (1995).
[10] V. Kumaran and R. Muralikrishnan, Phys. Rev. Lett. **84**, 3310 (2000).
[11] R. Muralikrishnan and V. Kumaran, Phys. Fluids **14**, 775 (2001).
[12] V. Shankar and V. Kumaran, J. Fluid Mech. **434**, 337 (2001).
[13] V. Shankar, J. Non-Newtonian Fluid Mech. **117**, 163 (2004).
[14] V. Gkanis and S. Kumar, Phys. Fluids **15**, 2864 (2003).
[15] V. Shankar and S. Kumar, J. Non-Newtonian Fluid Mech. **116**, 371 (2004).
[16] M. D. Eggert and S. Kumar, J. Colloid Interface Sci. **278**, 234 (2004).
[17] V. Gkanis and S. Kumar, J. Fluid Mech. **524**, 357 (2005).
[18] L. Srivatsan and V. Kumaran, J. Phys. II **7**, 947 (1997).
[19] V. Shankar and V. Kumaran, J. Fluid Mech. **407**, 291 (2000).
[20] M. Hamadiche and M. Gad-el-Hak, J. Fluids Struct. **16**, 331 (2002).
[21] V. Shankar and L. Kumar, Phys. Fluids **16**, 4426 (2004).
[22] G. Haacke, J. S. Brinen, and P. J. Larkin, J. Coat. Technol. **67**, 29 (1995).
[23] P. Krindel and A. Silberberg, J. Colloid Interface Sci. **71**, 39 (1979).
[24] P. W. Carpenter, A. D. Lucey, and C. Davies, J. Aircr. **38**, 504 (2001).
[25] M. Gad-el-Hak, in *Flow past Highly Compliant Boundaries and in Collapsible Tubes*, edited by P. W. Carpenter and T. J. Pedley (Kluwer, Dordrecht, 2003).
[26] K. S. Yeo, J. Fluid Mech. **196**, 359 (1988).
[27] A. E. Dixon, A. D. Lucey, and P. W. Carpenter, AIAA J. **32**, 256 (1994).